Scripta Materialia 155 (2018) 32–36

Contents lists available at ScienceDirect

Scripta Materialia

journal homepage: www.elsevier.com/locate/scriptamat

Regular article

Evaluation of thermal aging of δ-ferrite in austenitic stainless steel weld using nanopillar compression test

Ho Jung Lee [a], Byeong Seo Kong [b], Gokul Obulan Subramanian [b], Jaewon Heo [b], Changheui Jang [b,*], Kyoung-Soo Lee [a]

[a] Central Research Institute, Korea Hydro & Nuclear Power Co., Ltd, Daejeon, 34101, Republic of Korea
[b] Dept. of Nuclear and Quantum Engineering, Korea Advanced Institute of Science and Technology, Daejeon, 34141, Republic of Korea

ARTICLE INFO

Article history:
Received 16 March 2018
Received in revised form 26 April 2018
Accepted 7 June 2018
Available online xxxx

Keywords:
Thermal aging
δ-Ferrites
Spinodal decomposition
G phase
Nanopillar compression test

ABSTRACT

The effects of thermal aging on microstructure and mechanical property change of δ-ferrite in an austenitic stainless steel weld were investigated. After thermal aging at 400 °C for 20,000 h, spinodal decomposition and G phase precipitation were observed, along with ~80% increase in yield strength measured by nanopillar compression test. Subsequent reversion heat treatment removed spinodal decomposition while leaving G phase, resulting in partial recovery of hardening in δ-ferrite. It was estimated that ~60% of the hardening in the δ-ferrite of the aged specimen was attributed to spinodal decomposition and ~40% to G phase, respectively.

© 2018 Acta Materialia Inc. Published by Elsevier Ltd. All rights reserved.

Austenitic stainless steel welds (ASSWs) are widely present at the joints of various piping systems, including the primary coolant system in light water reactors (LWRs). The ASSWs used in LWRs are required to have duplex phase microstructure consisting of mostly γ-matrix and certain amount of δ-ferrite to provide high resistance to hot cracking and stress corrosion cracking [1, 2]. Despite these advantages, previous studies have demonstrated that the δ-ferrite phase is susceptible to thermal aging embrittlement after prolonged exposure to the LWR operating temperature of 288–320 °C, which is usually measured by loss of fracture toughness, impact energy, and tensile ductility [3–9]. The primarily reason of such property degradation is well recognized as a thermal aging induced microstructural evolution at nanometer-scale, such as spinodal decomposition (separation of δ-ferrite to Fe-rich α and Cr-rich α' phases) and G phase precipitation in δ-ferrite. Spinodal decomposition and G phase precipitation lead to an internal coherency stress field and interact with dislocation movement (increase in dislocation density), thereby significant hardening occurs in the δ-ferrite phase [9, 10]. The mechanical property degradation is, therefore, closely related to hardening of δ-ferrite. In this regards, assessment of the hardening behavior of δ-ferrite, along with its microstructural evolution, needs to be understood to predict long-term aging behaviors of the weld components in LWRs.

In order to evaluate thermal aging embrittlement of δ-ferrite surrounded by γ-matrix, micro/nano-indentation techniques have been often used for duplex stainless steels (DSSs) [11–13] and cast austenitic stainless steels (CASSs) [14–18], which have relatively large δ-ferrite (tens to hundreds μm). It has been generally observed that the hardness value of δ-ferrite increased with aging temperature and exposure duration in the temperature range of 300–450 °C while that of austenite remained almost constant. Also, there have been similar attempts to evaluate the δ-ferrite phase in ASSWs [7, 19, 20], however, the δ-ferrite particles in ASSWs are usually too small (2 μm or smaller) to be accurately measured by nano-indentation (typical indented width ~1 μm) as the measured hardness values would be affected by the surrounding γ-matrix. In this work, therefore, we aim to evaluate aging induced microstructural and mechanical property changes in the δ-ferrite of ASSW using smaller scale method. That is, the mechanical behavior of δ-ferrite after aging was measured using nanopillar compression test [21, 22] to eliminate the effect of γ-matrix on measurement. Further, the relative contribution of spinodal decomposition and G phase to mechanical property change was assessed by reevaluating the samples after reversion heat treatment (R-HT), which is known to recover the mechanical properties by dissolving the spinodal decomposition in the δ-ferrite [11, 14].

A block of 316 L ASSW was fabricated by building-up layers of weld deposits on a 316 L plate using gas tungsten arc welding (GTAW) method. Chemical composition of finished weld was Fe — 18.4Cr — 11.0Ni — 2.6Mo — 1.7Mn — 0.4Si — 0.008C (in wt%) by the inductively coupled plasma (ICP) method. The δ-ferrite content of 316 L

* Corresponding author.
E-mail addresses: leehojung@khnp.co.kr (H.J. Lee), assaultpc@kaist.ac.kr (B.S. Kong), gokul@kaist.ac.kr (G. Obulan Subramanian), jay1@kaist.ac.kr (J. Heo), chjang@kaist.ac.kr (C. Jang), leekys1003@khnp.co.kr (K.-S. Lee).

https://doi.org/10.1016/j.scriptamat.2018.06.016
1359-6462/© 2018 Acta Materialia Inc. Published by Elsevier Ltd. All rights reserved.

ASSW used in this study was 11–12 vol%, which was estimated by using Schaeffer diagram and also measured by phase fraction method. The weld block was electro-discharge machined to small pieces, which were thermally aged in air furnace at 400 °C for 20,000 h. In addition, some of 400 °C aged sample were additionally exposed to 550 °C for 1 h, which is known as a reversion heat treatment to remove spinodal decomposition [11, 17]. An accelerated aging condition (i.e., 400 °C, 20,000 h) was selected to simulate an extended lifetime aging at LWR operating temperature. Above this temperature, the mechanism of aging embrittlement would be more of nucleation and growth instead of spinodal decomposition [23]. Specimens for microstructure evaluation and mechanical tests were taken at the location at least 2 mm from the surface of the aged pieces to exclude any environmental effect during thermal aging.

For the evaluation of microstructural features, a transmission electron microscope (TEM, Titan cubed G2 60–300) equipped with energy-dispersive spectroscope (EDS) was used at 300 kV. The TEM samples were prepared by a focused ion beam (FIB, Helios Nanolab 450 F1) with areas of 5 × 5 μm and less than 100 nm in thickness. Elemental mapping on selected area (50 × 50 nm) was performed for 300 s and line scan (50 nm with 150 point) for 100 s. Moreover, high resolution TEM (HRTEM) images were used for phase identification by fast Fourier transform (FFT).

Fig. 1a and b is the inversed pole figure (IPF) images of δ-ferrite from electron backscatter diffraction (EBSD) analysis taken on the top and side of the weld block, respectively. The δ-ferrite regions are mostly in [001] orientation on the top surface while in [101] orientation on the side surface. In the 316 L ASSW, therefore, the δ-ferrite phase tends to be aligned in [101] along the welding direction and in [001] along the thickness direction.

For δ-ferrite nanopillar specimen preparation, small coupons with 3 mm in diameter and 2 mm in thickness were prepared from the top surface of blocks and the surface of each coupon was ground with # 4000 grit SiC paper. Then, an anodic dissolution technique was applied to selectively dissolve the austenite phase but leaving δ-ferrite phase [24]. Three electrode setup consisted of standard calomel reference electrode, graphite rod counter electrode, and coupon working electrode was used in a non-deaerated 3.6 N H_2SO_4 + 0.1 N NH_4SCN solution. When the potential was kept at −120 mV_{SCE} for 150 s, γ-matrix was mostly removed to the depth of 4–7 μm, leaving a network of δ-ferrite as shown in Fig. 2a. The selective austenite dissolution of austenite was confirmed by XRD analysis, which revealed disappearance of austenite diffraction peaks while leaving δ-ferrite peaks on selectively dissolved coupons (not shown in this paper). After choosing a δ-ferrite column, nanopillars with around 400 nm diameter and 1200 nm in height (1:3 aspect ratio) were machined (see Fig. 2b and c) using FIB (Helios Nanolab 450 F1). Then, the in-situ SEM uniaxial compression tests were carried out using a pico-indenter (Hysitron PI 85) equipped with 8 μm flat punch tip, which was installed in FIB (Quanta 3D FEG). Compression load was applied along [001] direction at a nominal displacement rate of $1 \times 10^{-3}\ s^{-1}$ up to 20% displacement. In each test condition, at least duplicated test results were obtained for the reproducibility of property data.

Fig. 3 shows the results of TEM analysis within the δ-ferrite of the as-welded, aged, and aged + reversion heat-treated (R-HTed) samples. First, in case of the as-welded 316 L ASSW, the TEM/EDS mixed mapping images show that major elements such as Fe, Cr, and Ni are rather uniformly distributed without any significant spatial enrichment in δ-ferrite as shown in Fig. 3a. Element profile in TEM/EDS line scan result (Fig. 3b) indicates small fluctuation in element concentration [average ± standard deviation (min. − max.)] of Fe, Cr, and Ni of 62.3 ± 1.1 (59.1–65.8), 23.3 ± 0.9 (21.2–26.2), and 5.7 ± 0.5 (4.4–6.8), respectively. Moreover, the fast Fourier transformation (FFT) pattern taken in TEM/EDS mapping region in Fig. 3a exhibits a body-centered cubic (BCC) structure of δ-ferrite without any secondary phases (Fig. 3c).

On the other hand, for the aged 316 L ASSW, separation of alloying elements at nanoscale is observed as shown in Fig. 3d and e. The TEM/EDS mixed mapping images indicate that the Cr-enriched region with a width of approximately 5 nm is distinguished from Fe- and Ni-enriched region. The TEM/EDS line scan result confirms that fluctuation in concentration of Fe, Cr, and Ni shows ranges of 64.3 ± 3.1 (53.0–67.7), 25.9 ± 2.9 (20.2–34.5), and 4.5 ± 1.3 (4.5–7.1), respectively. That is, the standard deviation of concentration, especially for Fe and Cr, increases around three times for aged specimen. Also, the fluctuation in element concentration (max. and min.) of aged specimen is much larger than those of as-welded specimen. Both seem to be caused by the separation of Fe- and Ni-rich α and Cr-rich α' domain in δ-ferrite. F. Danoix and P. Auger [25] reported that such separation

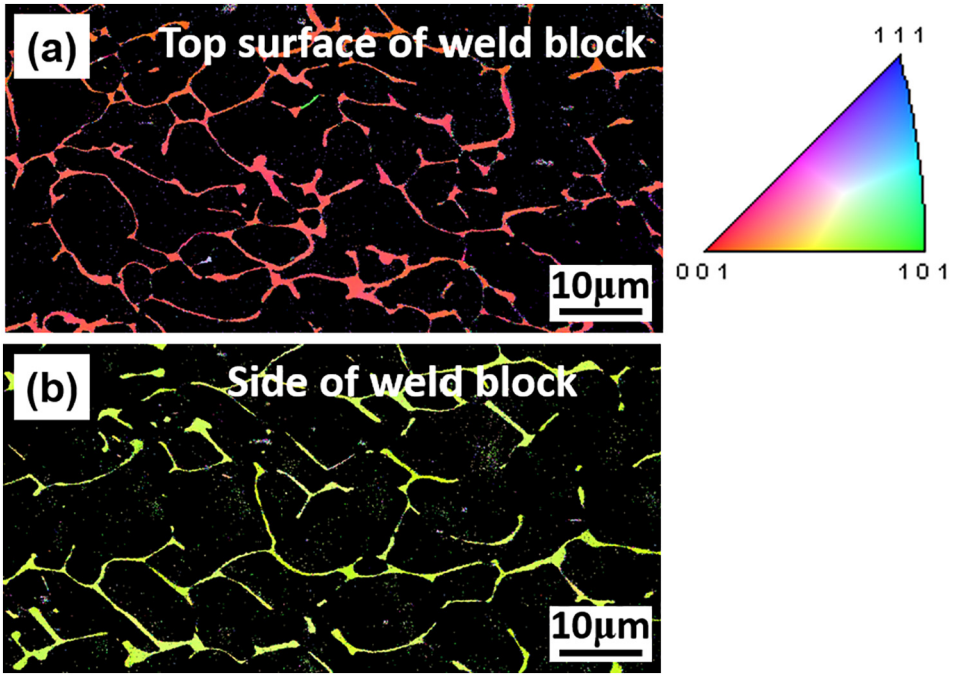

Fig. 1. EBSD IPF images of δ-ferrite in 316 L ASSW taken (a) on the top and (b) side of the weld block.

Download English Version:

https://daneshyari.com/en/article/7910198

Download Persian Version:

https://daneshyari.com/article/7910198

Daneshyari.com